Detection and Classification of Potential Caves on the Flank of Elysium Mons, Mars

Ravi Sharma[1] and Neeraj Srivastava[2]

[1] J.J.T. University, Jhunjhunu, Rajasthan 333001, India; science.rs08@gmail.com
[2] Planetary Science Division, Physical Research Laboratory, Ahmedabad 380009, India

Abstract

Martian caves have revived interest in the field of subsurface exploration because they are the potential destinations for future human habitats and astrobiological research. There are many pits on Mars, but some of them look like collapsed cave roofs. These special pits are formed by the collapse of surface materials into the subsurface void spaces. The signature of life is probable in a subsurface cave on Mars as the subsurface environment can protect life from the harsh and dangerous radiation environment of the surface. In a cave, there may be an abundance of minerals, fluids, and other key resources. Therefore, locating the access point of the subsurface cave is essential and crucial for formulating plans for robotic/human explorations of the Red Planet, Mars. We have used remote sensing data from Mars Reconnaissance Orbiter (MRO; NASA), Mars Global Surveyor (MGS; NASA), and Mars Odyssey (NASA) for identifying, mapping, and classifying selected special pit candidates on the flank of Elysium Mons, Mars. A total of 32 special pit candidates has been identified and classified based upon morphology and geological context. Out of these, 26 are newly discovered ones. The thermal behavior of 23 special pit candidates confirms that the special pits are radiating heat energy at nighttime, similar to potential caves. Also, cave entrances have been detected in nine candidates using data from the HiRISE camera onboard MRO. These sites could be important destinations for future robotic/human exploration and the search for life on Mars.

Key words: planets and satellites: individual (Mars) – planets and satellites: surfaces – planets and satellites: general

1. Introduction

There are many pits on Mars, but some of them look like collapsed cave roofs. Such a pit is an opening on the cave roof or ceiling to admit natural light. These pits are referred to as special pits in this study, and they form by the collapse of surface material into the subsurface void spaces. They can be associated with tube-fed lava flows, volcanic-tectonic features, or rille structures (Cushing 2012; Cushing et al. 2015). Sunlight enters the cave entrance zone from the access point of the pit, and very high-temperature fluctuation occurs in the portion that is directly illuminated. The surrounding areas in the twilight zone exhibit only minor temperature changes because they are illuminated only by scattered light.

Most importantly, the temperature in the un-illuminated part of the cave remains more-or-less constant. Therefore, there is the possibility of an abundance of ice and other cave resources in this zone (Boston et al. 2003a, 2003b; Hill & Forti 1997; Romero 2009; Bairagya 2014). The caves also protect from dust storms, high-energy ultraviolet radiations, and cosmic rays (Boston et al. 2004). Thus, the caves are potential sites for future robotic/human explorations of the surface of Mars (Boston et al. 2003b). Considering these aspects in this study, we have examined special pit candidates in the Elysium Mons region of

Mars with the help of existing data sets from various remote sensing missions. There are three proposed human exploration zones around Elysium Mons. These are Hebrus Valles (Davila et al. 2015), Phlegra Dorsa (Barker et al. 2015), and Cerberus Fossae (Wright et al. 2015). Therefore, it is possible that future human/rover-based exploration into the potential caves on Elysium Mons can discover critical resources.

Special pits were discovered on Mars in the year 2007 in the Tharsis region (Cushing et al. 2007). Cushing (2021) released an updated version of the Mars Cave Candidate Catalog, which includes 44 special pit candidates present on the flank of Elysium Mons. Out of these, we have included six candidates in this study for detailed morphometry and thermal examination. In addition, we searched for and characterized new special pits in the Elysium Mons region of Mars in this study using remote sensing data sets from Mars Reconnaissance Orbiter (MRO), Mars Global Surveyor (MGS), and Mars Odyssey missions of NASA.

2. Datasets Used

In this study, we used imaging data sets, spectrometer data, and altimetry data from several remote sensing missions to Mars by NASA. These include panchromatic data from High

Resolution Imaging Science Experiment (HiRISE) and Con-TeXt (CTX) camera from MRO (2005—present) (Malin et al. 2007), and THEMIS Infrared Projected Brightness Temperature (IRPBT) image data from Mars Odyssey (NASA) (Christensen et al. 2004; Christensen & THEMIS 2017). We also utilized Mars Orbiter Laser Altimeter (MOLA) data from MGS (NASA) (Smith et al. 2001, 2003). The spatial resolutions for these data sets are $\sim$0.25 m pixel^{-1} for HiRISE, $\sim$5–6 m pixel^{-1} for CTX, $\sim$100 m pixel^{-1} for THEMIS IRPBT, and $\sim$463 m pixel^{-1} for MOLA Mission Experiment Gridded Data Records (MEGDRs). The THEMIS IRPBT data are computed from Band 9 (12.57 μm) calibrated spectral radiance values assuming atmospheric opacity of 0.0 and surface emissivity of 1.0 (Christensen & THEMIS 2017). Apart from this, we also considered geological unit layers from Tanaka et al. (2014), and Mars Cave Catalog from Cushing & Okubo (2015), Cushing (2015), and Cushing (2019, 2021).

3. Methodology

3.1. Identification of Special Pit Candidates

Initially, CTX and/or HiRISE images were used to detect special pits based upon morphological investigations. As viewed from orbit, the special pits occur as a mostly circular structure having a collapsed cave roof and exhibiting a shadowed appearance in the un-illuminated part (Cushing et al. 2015). Unlike any impact craters, they are devoid of elevated rims, ejecta blanket, and rays (Figure 1). Further, the special pits show a warmer appearance than the surrounding area at nighttime (Cushing et al. 2015; Jung et al. 2014; Sharma et al. 2019; Sharma & Srivastava 2021) because heat from the outer surface is easily radiated while the loss of heat stored inside a cave is greatly inhibited and the cave radiates most of the heat energy through the special pits in nighttime (Antoine et al. 2009, 2011; Lopez et al. 2012), therefore special pits are considered as potential caves. We relied on the nighttime THEMIS infrared (IR) data of the northern summer season (Solar Longitude; Ls 90–180) for thermal observations. During the northern solar summer, the solar insolation is high, resulting in higher surface temperatures. Surface heat is a source of heat transferred to a subsurface cave. A greater amount of heat reaches the subsurface in the northern solar summer therefore the possibility of an excess amount of heat coming out from the special pit is also high. Hence, it is appropriate to consider the northern summer season data of the THEMIS IR observations. Here, "THEMIS IR" refers to the THEMIS Band-9 data (centered at 12.57 μm). Band-9 is useful because it detects surface brightness temperatures at a high signal-to-noise ratio (SNR) even at low temperatures. Primarily, the heat exchange between the subsurface caves and the outer surface occurs through the circulation of air (Cigna 1968). As per thermodynamics, heat flows from the direction of high temperature to low temperature (Boltzmann 1974). The temperature of the

surface of Mars drops steadily at night (Coblentz 1925; Fergason et al. 2006). At midnight, the difference in the temperature of the special pit and the surrounding area is maximum, therefore, it is appropriate to use the midnight data of the THEMIS IR observations.

We have restricted the extent of the surrounding area to a circular buffer zone of radius 500 m. The mid-nighttime temperature difference of the surrounding region (radius 500 m) of a special pit candidate T_D has been calculated by estimating the difference between the candidate special pit point location night-time maximum temperature ($T_{\max}$) and their average surrounding (radius 500 m) temperature ($T_{\mean}$). While estimating $T_{\mean}$ the temperature of the hotter pixel/ pixels has not been included. In most of the cases, we carried out thermal observations around midnight from $\sim$23:30 to 2:00. The thermal observation data of nighttime $\sim$21:00 to 22:00 were used in a few cases where midnight data were not available. The special pit shows a warmer appearance than the surrounding area, if $T_D > 0$. Apart from these, the temperature of the potential cave floor fluctuates with much lower diurnal amplitudes than the nearby surfaces (Cushing et al. 2015). Therefore, we calculated the diurnal amplitudes of the special pit candidate point location and the surrounding region. For this, $T_{\max}$, $T_{\mean}$, and T_D have been calculated for the thermal observations during the day (D) as well, around $\sim$13:00–14:00. Here, it is important to mention that the temperature data of the daytime and the nighttime for different special pit candidates are not corresponding to the same day on Mars.

3.2. Classification of Special Pit Candidates

3.2.1. Morphology

These special pit candidates are classified into types of Atypical Pit Craters (APCs) on the basis of morphology. According to Cushing et al. (2015), the APC I type candidates are bell-shaped and they possess overhanging walls and rims. The overhanging rim is thinner on the surface and thicker with increasing depth. If the overhang is symmetrical around the pit, the diameter of the cave floor may be approximately double that of the surface aperture. The APC II candidates show near-vertical walls for the upper part and overhanging walls in the lower part. The APC IIIs possess near-vertical walls with the absence of overhanging walls. Mostly, the APC Is possess a flat cave floor, and the talus material is absent in them. The APC IIs have a bowl-shaped cave floor with the presence of talus material, and APC IIIs have a flat cave floor with dust-covered rubble. Thus, the lateral extent of the overhanging walls decreases in APC IIs in comparison to APC Is. It can be noted that APC IIs may be misinterpreted as APC IIIs in nadir observations unless the presence of overhangs at the base of pit walls is evident (Cushing et al. 2015).

We have estimated their true vertical depth at the point located at the edge of the shadow. The depths (D) of the special
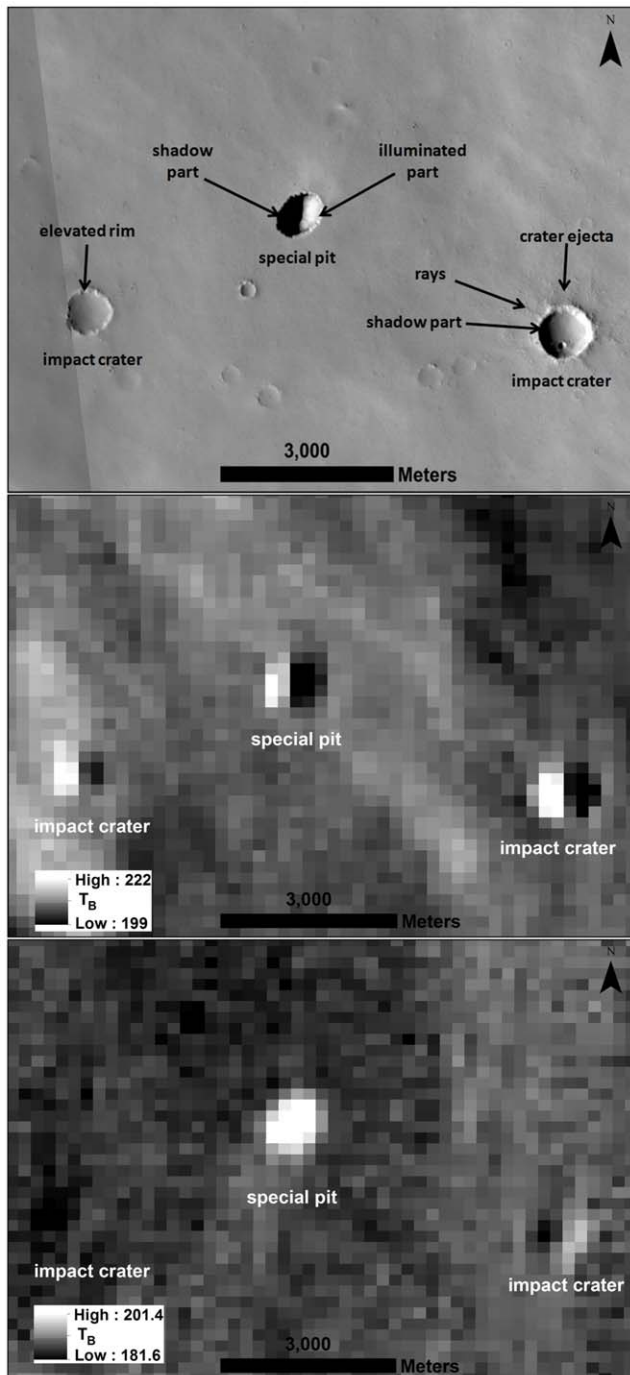
Figure 1. (a) A CTX daytime image (P02_001989_2077) (location 27.6947, 142.1096) acquired at 10:33 AM. (b) An IRPBT image taken during the evening at 5:22 PM. (c) An IRPBT image acquired at midnight around 11:34 PM.

pit candidates have been estimated from the length of shadows (Ls), the solar incidence angle (i), and the emission angle (e) at the time of the observation, using the approach of Cushing et al. (2015). Formulas $D = \text{Ls}/[\tan(i) - \tan(e)]$ and $D = \text{Ls}$

$\cos(i)\cos(e)/[\sin(i+e)]$ were applied to calculate the depth of the special pit candidates for Phase Angle $<i$ and Phase Angle $>i$, respectively. Here, the length of the visible shadow (Ls) is the horizontal distance in the direction of illumination from the shadow-casting point on the rim to the edge of the shadow cast upon the floor, and depth (D) is the true vertical depth at that point.

3.2.2. Geological Context

Besides the morphometric characterization of the special pits, we have also classified them based on their formation mechanism and geological context. The nature of the origin of the pits in this study should be mostly volcanic or tectonic since they are situated on the flank of Elysium Mons. During volcanism, there is a movement of magma in the subsurface and lava on the surface. Both these activities can result in the formation of pits due to different processes.

(i) Lava Tubes (LTs)—Low-viscosity lava flows on the surface. The upper layer of the lava flow cools relatively faster. Therefore, the top layer hardens, which results in the formation of a tube. The rapid flow of lava through the tube decreases with time, and finally, the tube is left with no lava flow. The empty tube would have hard boundaries and space inside (Valerio et al. 2008). If the roof of this tube collapses, a special pit is formed, which provides access to the LT cave.

(ii) Horizontal Magma Conduit (HMC)—The horizontal propagation of magma through flank conduits form an HMC. The subsurface flow of magma forms the underground tubes (Neri 2010). The overhead material of this tube can fall due to tectonic activities, which results in the formation of a special pit that is connected to the subsurface tube. In this case, only the pit would be visible, and no tube would be observed on the surface.

(iii) Tectonic Feature (TF)—The region with a high influx of subsurface magma flow would have a large tectonic activity that results in the formation of rift zones. The strong tectonic activities in the rift zone can produce faults and grabens. In these cases, the pits are associated with visibly discernible TFs on the surface. On most occasions, these pit candidates form a chain (Cushing et al. 2015).

The special pit candidates have been classified as LT special pits when they are associated with LTs, and candidates have been classified as TF special pits when they are associated with fractures, faults, or graben. If the special pit candidates are located on a volcanic flank but are not associated with either LT or TFs, they are classified as HMC special pits.

3.3. Determination of Potential Cave Entrance

Determining potential cave entrances is very useful for future crewed or robotic exploration of the Red Planet, Mars. In the HiRISE images, the darker black area represents potentially greater depths where the sunlight is barely reaching. In this
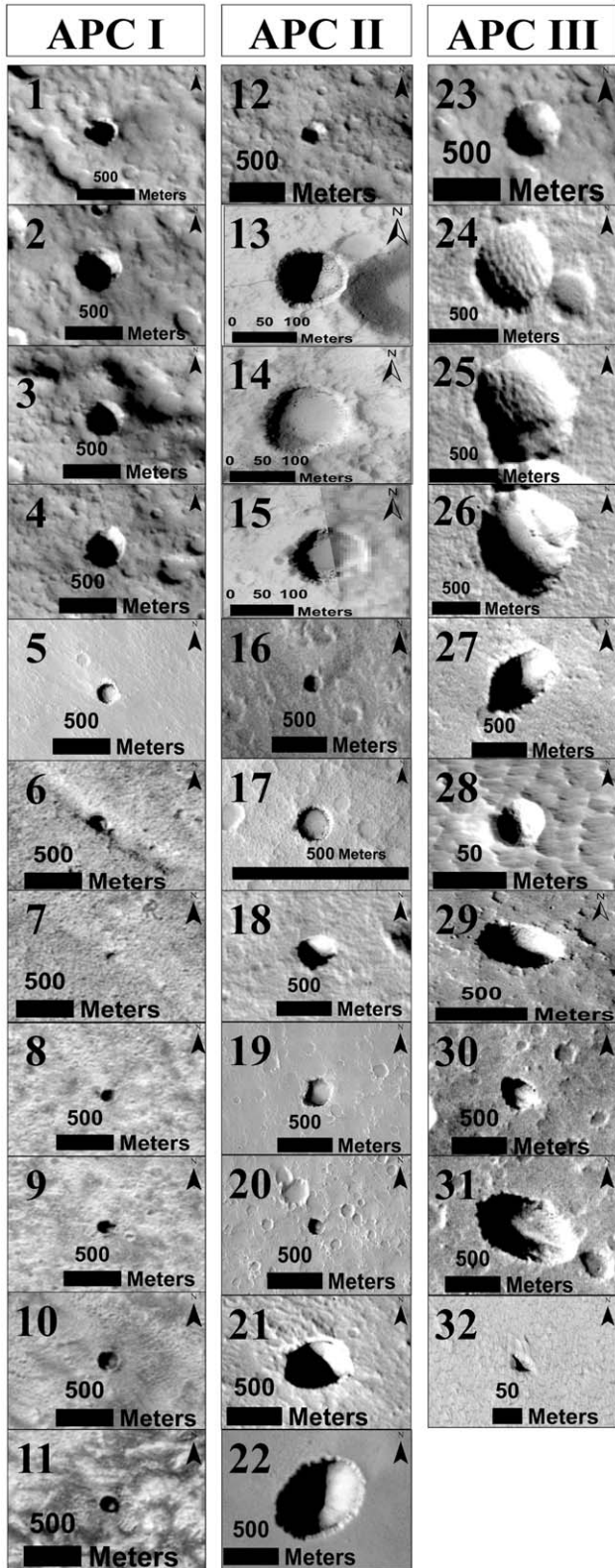
Figure 2. A view of the 32 special pits using CTX/HiRISE images. SP 1−11, SP 12–22, and SP 23–32 have been classified into APC I, APC II, and APC III respectively.
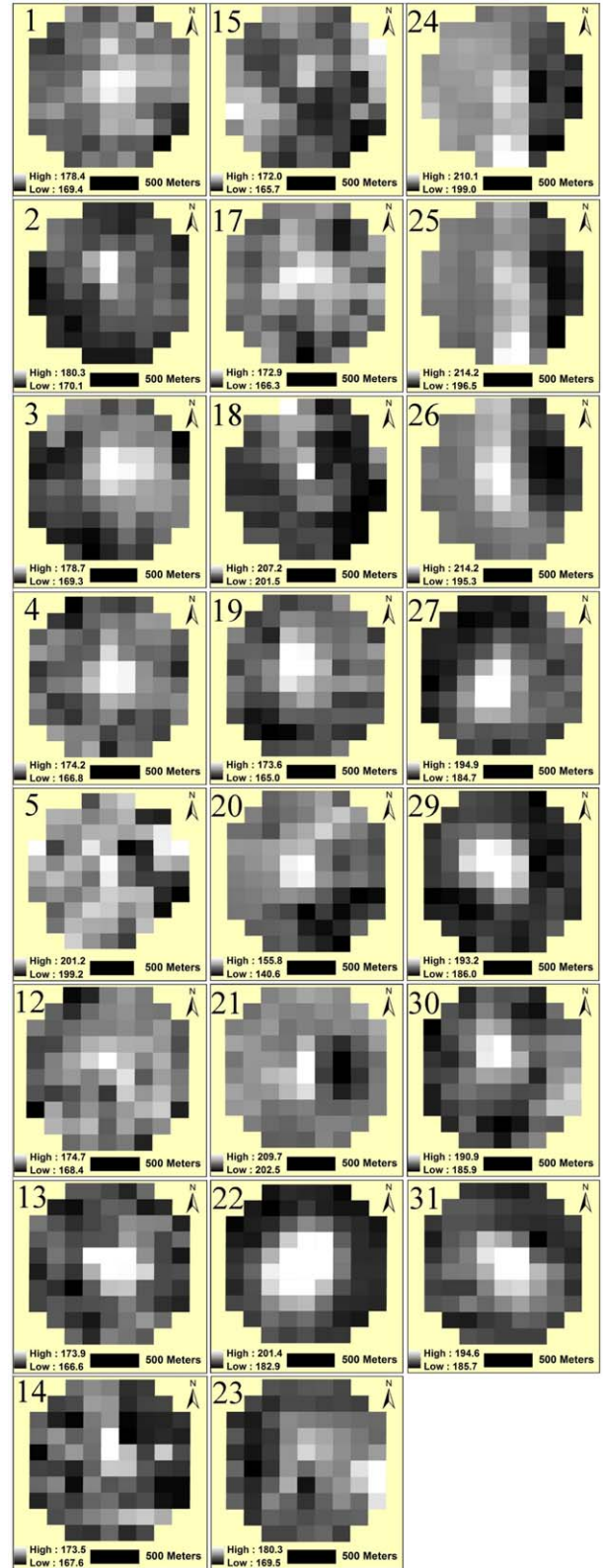

Figure 3. A view of the THEMIS IRPBT images of 23 special pits. The SP 6–11, 16, 28, and 32 are less than 100 m in diameter therefore their thermal behavior could not be studied.

Table 1
Morphology, Geological Context, and Thermal Observation of Special Pits

Morphology	Identification no., SP	Location Latitude Longitude	Elevation (m)	Geological Context GU	AGF	Time	Thermal Observation IRPBT	T_{max}	T_{mean}	Newly Discovered Special Pits in this Study
APC I	1	24.4781 147.1324	11556	Hve	LT	N	i63410018	178.4	173.1	New
						D	i55523012	189.8	186.7	
	2	24.4458 147.1225	11436	Hve	⋯	N	i63410018	180.3	173.5	New
						D	i55523012	192.9	187.1	
	3	24.7341 147.3604	9912	Hve	LT	N	i54618008	178.7	172.8	New
						D	i55523012	193.2	190.2	
	4	24.5934 147.4581	9208	Hve	⋯	N	i55979006	174.2	167.3	New
						D	i55523012	196.3	191.7	
	5	29.2600 145.6594	−224	AHv	⋯	N	i54337020	201.1	200.4	MCC
						D	⋯	⋯	⋯	
	6	30.585 140.238	−2193	AHv	TF	N	i64502029	⋯	⋯	New
						D	⋯	⋯	⋯	
	7	30.5963 140.2247	−2220	AHv	TF	N	i64502029	⋯	⋯	New
						D	⋯	⋯	⋯	
	8	30.9681 140.2599	−2532	AHv	⋯	N	i64502029	⋯	⋯	New
						D	⋯	⋯	⋯	
	9	30.9834 140.3423	−2547	AHv	⋯	N	i55773011	⋯	⋯	New
						D	⋯	⋯	⋯	
	10	31.0412 140.5132	−2551	AHv	⋯	N	i64502029	⋯	⋯	New
						D	⋯	⋯	⋯	
	11	31.0132 140.3454	−2555	AHv	⋯	N	i64502029	⋯	⋯	New
						D	⋯	⋯	⋯	
APC II	12	24.4439 147.4351	9265	Hve	⋯	N	i54618008	174.7	171.5	New
						D	i55523012	190.7	190.6	
	13	24.7541 147.5137	8919	Hve	⋯	N	i55979006	173.9	168.8	MCC
						D	i55523012	193.1	190.2	
	14	24.7602 147.5456	8706	Hve	⋯	N	i55979006	173.5	169.1	New
						D	i55523012	190.5	190	
	15	24.7667 147.5712	8472	Hve	⋯	N	i55979006	172	168.3	New
						D	i55523012	193.2	190	
	16	25.5711 146.4503	7512	Hve	⋯	N	i56004005	⋯	⋯	New
						D	⋯	⋯	⋯	
	17	24.4158 150.6179	4050	Hve	⋯	N	i54593008	172.9	169.3	MCC
						D	⋯	⋯	⋯	
	18	25.0786 144.6775	2438	Hve	⋯	N	i63217009	206.2	202.8	New
						D	⋯	⋯	⋯	
	19	22.5202 149.8417	2368	Hve	⋯	N	i54618008	173.6	168	MCC
						D	i63903010	207.3	203.2	
	20	23.2104 151.7289	2034	AHv	⋯	N	i55005012	155.8	146.8	MCC
						D	i71149006	204.9	203.4	
	21	26.3785 144.1544	1828	Hve	⋯	N	i63217009	209.7	205.8	New
						D	⋯	⋯	⋯	
	22	27.6947 142.1096	710	AHv	⋯	N	i55698010	201.4	186.1	New
						D	i62749014	189.4	184.5	
APC III	23	24.4488 147.1139	11495	Hve	⋯	N	i63410018	176.4	169.5	New
						D	i55523012	186.7	186.4	
	24	25.1059 144.6727	2468	Hve	⋯	N	i63217009	207.8	203.9	New
						D	⋯	⋯	⋯	
	25	25.0977 144.6739	2462	Hve	⋯	N	i63217009	210.1	200.8	New
						D	⋯	⋯	⋯	
	26	25.0892 144.6751	2447	Hve	⋯	N	i63217009	214.2	203	New
						D	⋯	⋯	⋯	
	27	26.8415 142.2201	1072	IHvf	⋯	N	i55698010	194.9	187.3	New
						D	i62749014	186	182.2	
	28	19.8542 141.8167	667	AHv	⋯	N	i64246013	⋯	⋯	New
						D	⋯	⋯	⋯	

Table 1
(Continued)

| Morphology | Identification no., | Location | | Geological Context | | | Thermal Observation | | | Newly Discovered |
	SP	Latitude Longitude	Elevation (m)	GU	AGF	Time	IRPBT	$T_{\max}$	$T_{\mean}$	Special Pits in this Study
	29	22.9848 152.2478	186	AHv	⋯	N D	i63809022 ⋯	193.2 ⋯	187.2 ⋯	New
	30	22.9114 152.3603	129	AHv	⋯	N D	i63809022 ⋯	190.9 ⋯	187.4 ⋯	New
	31	22.9058 152.3724	124	AHv	⋯	N D	i63809022 ⋯	194.6 ⋯	188.2 ⋯	New
	32	30.5613 146.498	−1522	AHv	⋯	N D	i54362025 ⋯	⋯ ⋯	⋯ ⋯	MCC

Note. Here, SP, GU, Hve, IHvf, AHv, AGF, LT, TF, and MCC refer to Special Pits, geological units from Tanaka et al. (2014), Hesperian volcanic edifice, Late Hesperian volcanic field, Amazonian and Hesperian volcanic unit, associated geological features, LT, TFs, and Mars Cave Candidate Catalog (Cushing et al. 2015; Cushing & Okubo 2015; Cushing 2015, 2019, 2021) respectively. Here, if the associated geological feature for a special pit is neither an LT nor a TF, it might be associated with a subsurface HMC. Additional information, attributes of the special pits such as perimeter (Pe), maximum length ($L_{\max}$), maximum width ($W_{\max}$), and depth are tabulated in Table ST1. Here, the special pit's point location maximum temperature ($T_{\max}$) and their surrounding 500 m radius buffer zone mean temperature ($T_{\mean}$) have been calculated for the thermal observation time of day (D) and night (N) at the time period of ∼13:00–14:00 and ∼23:30-02:00 respectively. The thermal observation data of nighttime ∼21:00 to 22:00 were used in a few cases (SP 20, 29-31) where midnight data were not available. The IRPBT data from Mars Odyssey (Christensen et al. 2004; Christensen & THEMIS 2017) were downloaded through the publicly accessible web portal—Mars Orbital Data Explorer (ODE) (https://ode.rsl.wustl.edu/Mars/) provided by the PDS Geosciences Node at Washington University in St. Louis.
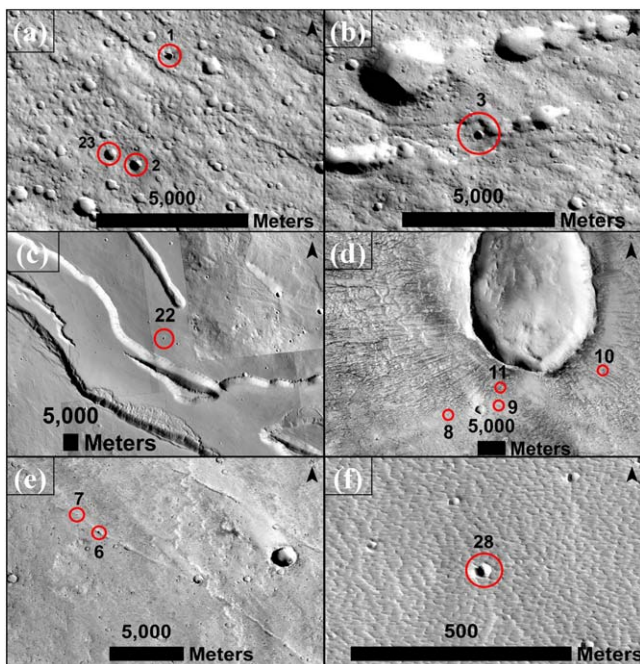

Figure 4. A view of the geological features associated with special pits. (a) A rille associated with SP 1 and presence of SP 2 and SP 23 in the nearby area; (b) a rille associated with SP 3; (c) SP 22 is located on a lava plateau, adjacent to a TF; (d) a large crater associated with SP 8, 9, 10, and 11; (e) a tectonic fracture associated with SP 6 and SP 7; and (f) a dune covering the volcanic field associated with SP 28.

region, there is a high probability of having a cave entrance. In general, the special pits exhibit potential cave entrance appearance as a dark linear part in the subset of the darker region when stretching the image contrast. First, the HiRISE darker region should limit its contrast range to low-end radiation values. This image shows a potential cave entrance as a dark area (Cushing et al. 2015).

4. Results and Discussion

4.1. Identification of Special Pit Candidates

We surveyed CTX and HiRISE images of the Elysium Mons region and found a lot of impact craters and pits in it. We were interested in finding special pits that looked like they were formed from the collapsed roof of the cave. Such special pits give a much darker look than the normal pits. They also have different morphological and thermal characteristics. An example of the morphological and thermal analysis of pit 22 in this study is provided in Figure 1. In the middle part of the image, there is a special pit candidate (SP 22). It can be seen that the impact craters in the adjoining areas exhibit crater rays, ejecta, and elevated rims, but the candidate special pit does not manifest any of these features (Figure 1(a)). Again, while in the THEMIS brightness temperature image of evening time, the candidate special pit and impact craters look alike (Figure 1(b)), and the special pit candidate displays a warmer
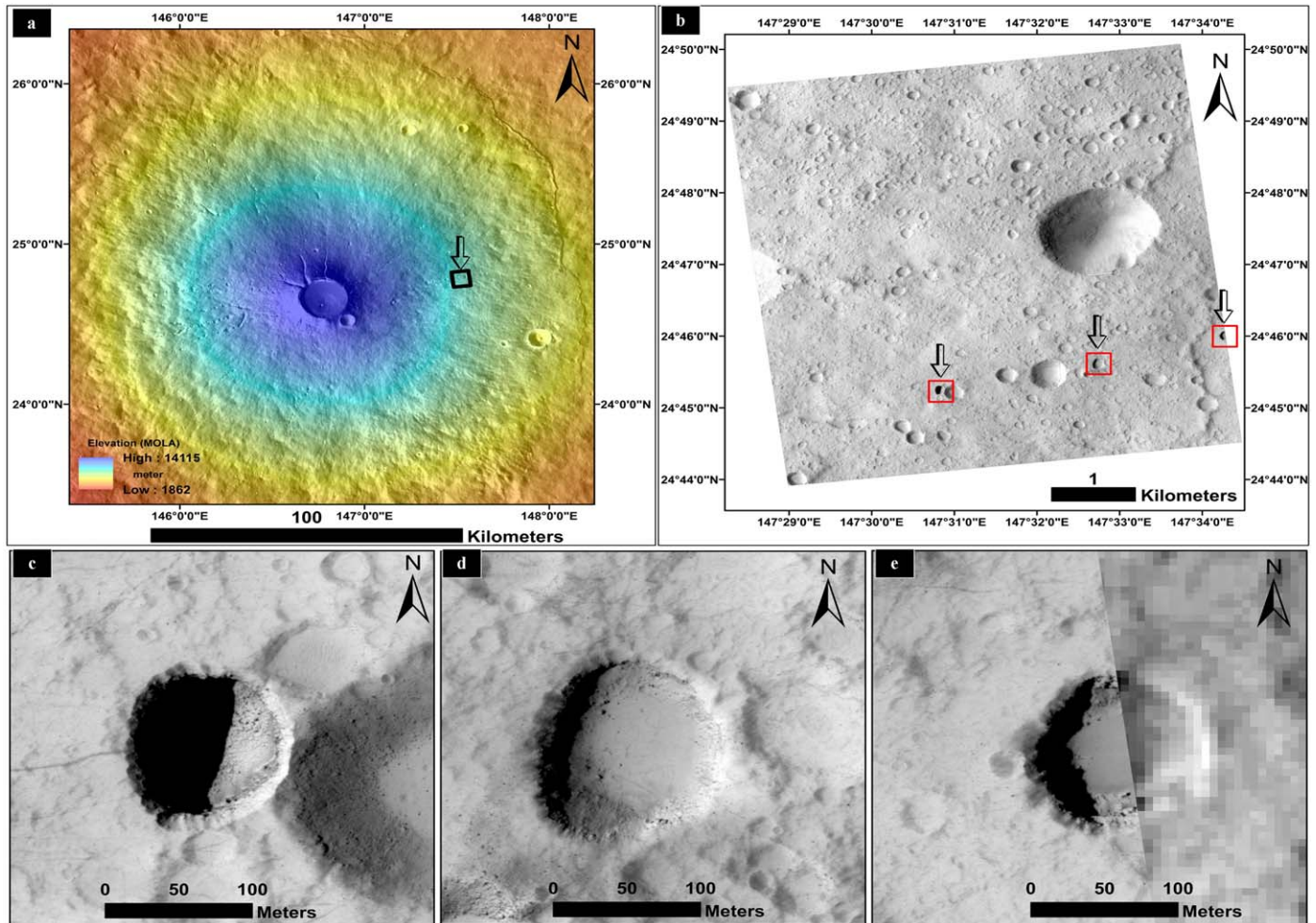
Figure 5. (a) Elevation map of the Elysium Mons region using MOLA and THEMIS IR day images in the background showing the location of the special pit (SP 13, SP 14, and SP 15); (b) Close-up view of the area enclosed by the black box in (a). Here, the individual special pits are enclosed by a red box. (c)–(e) Close-up views of the individual special pits. The sub-sections (c) and (d) have been prepared utilizing HiRISE images, while a combination of HiRISE (left side) and CTX (right side) data has been used for generating a close-up view of the third special pit (e).

appearance than the impact craters and the surrounding areas at midnight (Figure 1(c)). Further, it has been found that the SP 22 is 4.9 K warmer than the surrounding area in the daytime, whereas it is 15.3 K warmer than the surrounding area in the nighttime. Also, the diurnal amplitude of temperature variation for SP 22 is 10.4 K, which is much lower than the diurnal amplitude of temperature variation of the surrounding area (Figure 1(c)). SP 22 features morphological and thermal characteristics of a special pit; therefore, it is a potential access point of the cave.

Similarly, based on morphological and thermal characteristics, we have identified 32 special pit candidates on the flank of Elysium Mons (Figures 2 and 3). Among them, 26 candidates (SP 1−4, 6–12, 14–16, 18, and 21–31) are newly found ones, and the remaining six (5, 13, 17, 19–20, 32) are from the Mars Cave database of Cushing & Okubo (2015);

Cushing (2015), and Cushing (2019, 2021). The special pits SP 1–5, 12–15, 17–27, and 29–31 display a warmer appearance than the surrounding area (a circular buffer zone of radius 500 m) around midnight (11:30 pm to 2:00 am) in the northern summer season (Ls = 90–180). Since the midnight data were not available for four special pits (SP 20, 29–31), they were observed around 9–10 pm. Their location, elevation, geological context, and thermal observations are listed in Table 1.

4.2. Classification of Special Pits

4.2.1. Morphology

The special pits have been classified into APC I, APC II, and APC III as described in the methodology. As shown in Figure 2, SP 1–11 appear bell–shaped and have overhanging walls and rims; therefore, they are classified as APC I. The
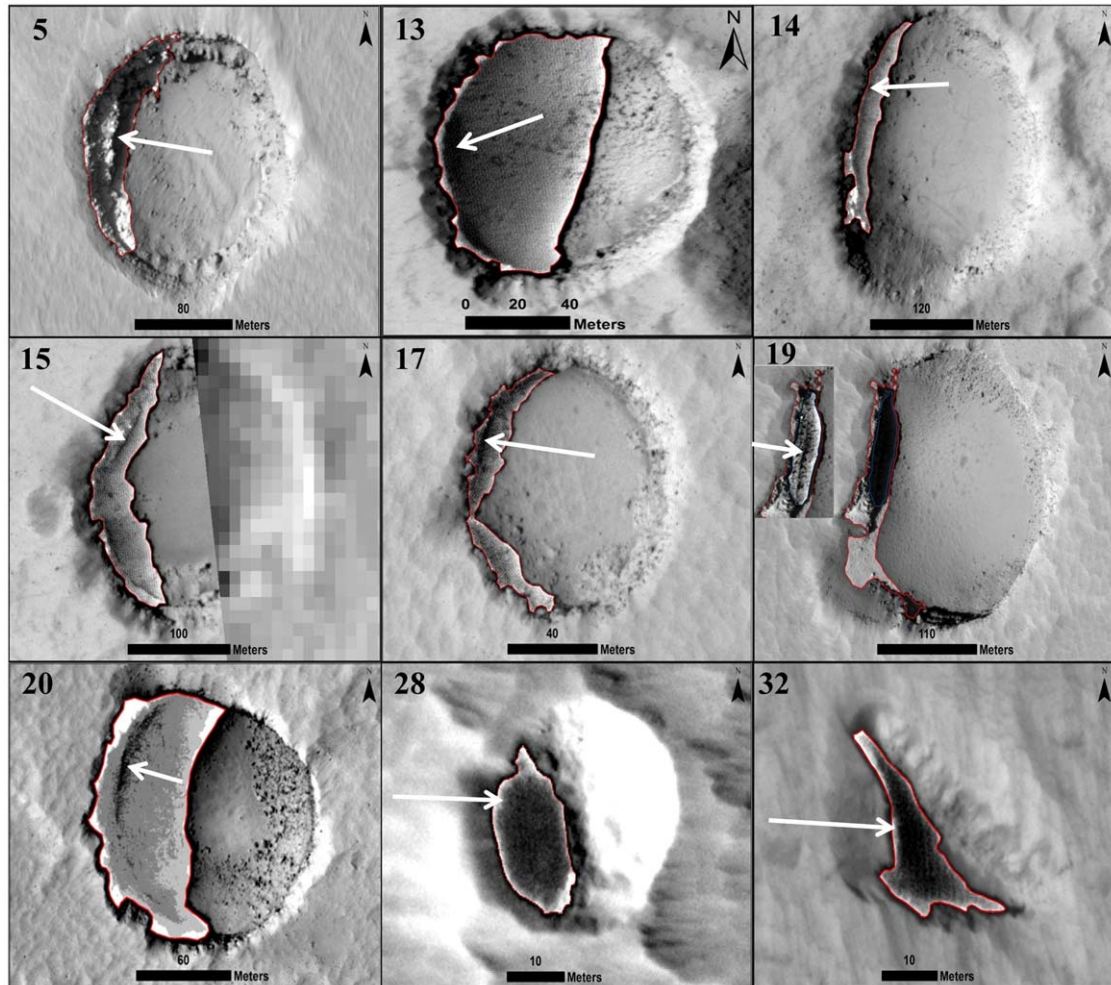
Figure 6. The contrast stretched HiRISE images of special pits (5, 13–15, 17, 19, 20, 28, and 32). The shadowed area in the original panchromatic images is enclosed by a red polygon. The white arrows show the potential entrance for the associated potential caves in each of these cases.

APC I cases are very deep, e.g., SP 5 and SP 6, and have calculated depths of ~493 m and ~100 m respectively. The area, perimeter, length, width, and depth of the special pits are tabulated in Table ST1. In SP 12−22, the walls appear to be near-vertical in the upper part; therefore, they are classified as APC II. There is a possibility of overhanging walls in the lower part. The special pits SP 23−32 possess near-vertical walls with the absence of overhanging walls; therefore, they are classified as APC III. APC IIIs appear to have heavy dust-covered rubble, e.g., SP 24–31.

4.2.2. Geological Context

This study demonstrates that two special pits, SP 1 and 3, are associated with LT rille structure (Figure 4(a), (b)); therefore, they are considered as LT special pits, whereas two special pits, SP 6 and 7, are associated with TFs (Figure 4(c), (e)) and

therefore are considered as TF special pits. The rest of the special pits are located on a volcanic flank but are not associated with LT and TFs; therefore, they are classified as HMC special pits, e.g., three special pits SP 13, SP 14, and SP 15. They are arranged in a linear array (Figure 5). It is possible that they may be related to the horizontal spread of magma through a flank conduit. SP 22 is located on a lava plateau, so it may be associated with the HMC. At the same time, it also has a nearby TF indicating that tectonic activity also contributed to the formation of this HMC special pit.

4.3. Determination of Potential Cave Entrance

CTX images (Figure SF1 (a) and Figure SF1 (b)) from different Sun incidence angles (Table ST2) of the special pit candidates have been studied on the flank of Elysium Mons. In all the images, the studied candidates exhibit morphological
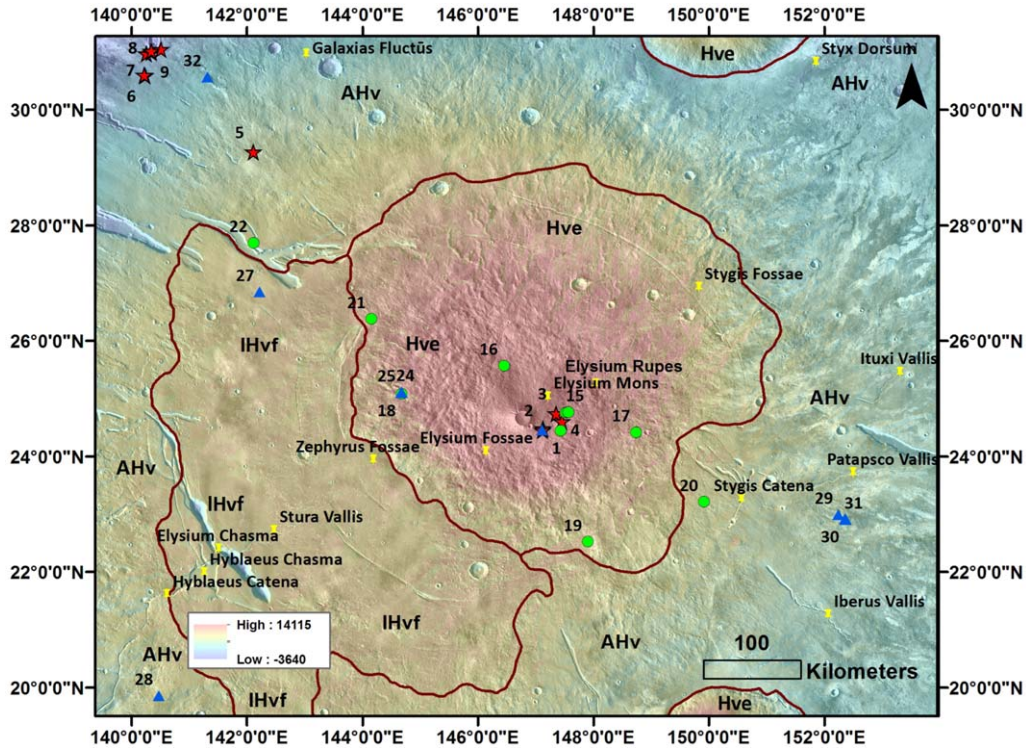
Figure 7. An elevation map of Elysium Mons, Mars from MOLA data showing the location of the 32 special pits studied here. The red stars, green dots, and blue triangles correspond to those classified as APC I (SP 1−11), APC II (SP 12−22), and APC III (SP 23−32), respectively. Out of 32 special pits, 26 SPs (SP 1−4, 6−12, 14−16, 18, and 21−31) are newly discovered ones. The name of the geological location is indicated by the label with a yellow pin.

characteristics of special pits. At different Sun incidence angles, the shadowed portion of the special pit candidates gets reduced or enhanced; however, it has been observed that a portion of the special pit candidates consistently appear dark in all the images suggesting that this constantly dark appearing area is very deep where sunlight does not reach. It is very likely that the cave entrance is present in this dark zone.

The determination of a potential cave entrance is possible using HiRISE images (Figure 6 and Table ST3) due to its very high spatial and radiometric resolution. In this study, investigation for a potential cave entrance has been attempted for nine special pits for which HiRISE images were available. As shown in Figure 6, a subset of the shadowed part in the contrast stretched HiRISE images is delineated by the red boundary. The long shadows beneath the layers indicate an "overhang" where possible entrances to a cave may occur as other entrances are not detected elsewhere in the walls of the pits at the current image resolution. In this region, there is a high probability of the presence of a cave entrance. The SK 5, 13–15, 17, and 19–20 exhibit potential cave entrance in the form of a dark linear part indicated by a white arrow (Figure 6). The gray and relatively white areas are shallower regions on the potential cave floor where the scattered sunlight is reaching. The reduction of depth in these areas of the potential cave floor

may be due to the presence of talus and/or dust material of varying thicknesses. The white areas have a thicker pile compared to the gray areas. In most of these cases, the white area is also found at the edges of the subset since the light directly reaches the edges or the sides of the upper walls.

SP 28 and SP 32 exhibit a potential cave entrance in the form of a continuous shadowed pattern. The white pattern is visible at the edges of the upper walls with a continuous shadow pattern on the potential cave floor which indicates that the upper roof of the rock shelter has suddenly collapsed or a huge amount of dust has fallen. In SP 5, heavy talus material has been observed as a white pattern in the west and southwest directions, while gray shade indicates irregular collapse material on the potential cave floor during different times. SP 14 and SP 19 have a pile of talus material in the southwest and western directions signified by a white dotted scattered pattern. Comparatively less, SP 15 has a pile of talus material in the northwest and western directions. In SP 19, the darker region is present in the northwest and west directions as it is indicative of higher depth, while the subset of the darker region in an enclosed box on the left side is indicative of the irregular pile of talus material and dust at the potential cave floor that accumulates over time. Thus, the HiRISE image investigation also indicates the evolutionary stage of special pits by

providing evidence for the presence of dust and talus material on the potential cave floor.

5. Conclusions

In this study, 32 special pit candidates on the flank of Elysium Mons on Mars (Figure 7) have been classified on the basis of morphology and geological context. Out of these, 26 special pit candidates (SP 1–4, 6–12, 14–16, 18, and 21–31) are newly identified ones. Among all, based upon their morphology, 11 candidates (SP 1−11) have been classified as APC Is, 11 candidates (SP 12–22) as APC IIs, and 10 candidates (SP 23–32) as APC IIIs. Two of the special pit candidates are associated with LTs and two with TFs; therefore, they are considered as LT special pits and TF special pits, respectively. Others could be associated with HMCs. Consequently, they have been classified as HMC—special pits. In addition to their geological setting, the potential cave entrances have been worked out for the candidates for which HiRISE data were available. Our thermal investigations have revealed that the special pits identified in this study are radiating heat at night, similar to the potential caves. Thus, the special pit candidates in this study could be suggestive of possible caves on the flanks of Elysium Mons, which could be essential destinations for future human/rover missions as well as the search for life on Mars.

ORCID iDs

Ravi Sharma ⓘ https://orcid.org/0000-0002-3522-4077

References

Antoine, R., Baratoux, D., Rabinowicz, M., et al. 2009, JVGR, 183, 228
Antoine, R., Lopez, T., Baratoux, D., Rabinowicz, M., & Kurita, K. 2011, Icar, 214, 433
Bairagya, H. 2014, International Journal of Environment, 3, 150
Barker, D. C., James, G., Chamitoff, G., & Clifford, S. 2015, in First Landing Site/Exploration Zone Workshop for Human Missions to the Surface of Mars, LPI Contributions, Vol. 1879 (27-30 Oct. 2015) (Lunar and Planetary Institute: Houston, TX), 1002
Boltzmann, L. 1974, The Second Law of Thermodynamics (Berlin: Springer), 13
Boston, P., Frederick, R., Hildreth-Werker, V., et al. 2003a, Human Utilization of Subsurface Extraterrestrial Environments: Final Report, NIAC – Caves of Mars (Tampa, FL: University of South Florida, Complex System Research, Incorporated, and NASA Institute for Advanced Concepts)
Boston, P., Frederick, R., Welch, S., et al. 2003b, Gravit. Space Biol. Bull., 16, 121
Boston, P. J., Frederick, R. D., Welch, S. M., et al. 2004, in AIP Conf. Ser., 699, Space Technology and Applications, ed. M. S. El-Genk (Melville, NY: AIP), 1007
Christensen, P. R., Jakosky, B. M., Kieffer, H. H., et al. 2004, SSRv, 110, 85
THEMIS, Christensen, P. R. 2017, 2001 Mars Odyssey Thermal Emission Imaging System (THEMIS), Data Processing User's Guide Part 1 Infrared, Version 0.23, https://static.mars.asu.edu/pds/ODTSDP_v1/calib/process_ir.pdf
Cigna, A. A. 1968, International Journal of Speleology, 3, 3
Coblentz, W. W. 1925, AN, 224, 361
Cushing, G. 2012, Journal of Cave and Karst Studies, 74, 33
Cushing, G. 2015, Mars Global Cave Candidate Catalog PDS4 Archive Bundle. PDS Cartography and Imaging Sciences Node (IMG)
Cushing, G. 2019, Mars Global Cave Candidate (MGĈ3) v1 cushing,USGS Astrogeology Science Center
Cushing, G. 2021, Mars Global Cave Candidate (MGĈ3) v1 cushing, USGS Astrogeology Science Center
Cushing, G. E., & Okubo, C. H. 2015, in Int. Planetary Caves Conf., LPI Contributions, 1883 (20-23 Oct. 2015) (Flagstaff, AZ: Lunar and Planetary Institute), 9026
Cushing, G. E., Okubo, C. H., & Titus, T. N. 2015, JGRE, 120, 1023
Cushing, G. E., Titus, T. N., Wynne, J. J., & Christensen, P. R. 2007, GeoRL, 34, 17201
Davila, A., Fairén, A. G., Rodríguez, A. P., et al. 2015, in First Landing Site/Exploration Zone Workshop for Human Missions to the Surface of Mars, LPI Contributions, Vol. 1879 (27-30 Oct. 2015) (Houston, TX: Lunar and Planetary Institute), 1012
Fergason, R. L., Christensen, P. R., & Kieffer, H. H. 2006, JGRE, 111, E12004
Hill, C., & Forti, P. 1997, Cave Minerals of the World (2nd edn.; Huntsville, AL: National Speleological Society), 463
Jung, J., Yi, Y., & Kim, E. 2014, JASS, 31, 141
Lopez, T., Antoine, R., Baratoux, D., et al. 2012, JGRE, 117, E09007
Malin, M. C., Bell, J. F., Cantor, B. A., et al. 2007, JGRE, 112, E05S04
Neri, M. 2010, Acta Borealia, 22, 53
Romero, A. 2009, Cave Biology: Life in Darkness (Cambridge: Cambridge Univ. Press)
Sharma, R., & Srivastava, N. 2021, Earth and Space Science Open Archive (ESSOAr), 25, https://doi.org/10.1002/essoar.10506123.1
Sharma, R., Srivastava, N., & Yadav, S. K. 2019, RAA, 19, 116
Smith, D. E., Zuber, M. T., Frey, H. V., et al. 2001, JGRE, 106, 23689
Smith, D. E., Zuber, M. T., Neumann, G. A., Guinness, E. A., & Slavney, S. 2003, Mars Global Surveyor Laser Altimeter Mission Experiment Gridded Data Record, MGS-M-MOLA-5-MEGDR-L3-V1.0, NASA Planetary Data System, 2003
Tanaka, K. L., Skinner, J. A. J., Dohm, J. M., et al. 2014, U.S. Geological Survey Report, 3292
Valerio, A., Tallarico, A., & Dragoni, M. 2008, JGRB, 113, B08209
Wright, S. P., Niles, P. B., Bell, M. S., et al. 2015, in First Landing Site/Exploration Zone Workshop for Human Missions to the Surface of Mars, LPI Contributions, Vol. 1879 27-30 Oct. 2015 (Houston, TX: Lunar and Planetary Institute), 1017